NANO LETTERS

pubs.acs.org/NanoLett Letter

# Modulation of Semiconductor Quantum Dot Photoluminescence by Photochromic Molecules

Heyou Zhang, Pankaj Dharpure, Arun Ashokan, Max Gießübel, Paul Mulvaney, Mukundan Thelakkat, and Jürgen Köhler*

Cite This: https://doi.org/10.1021/acs.nanolett.5c06282 Read Online

ACCESS | Metrics & More | Article Recommendations | Supporting Information

**ABSTRACT:** A hybrid system comprising semiconductor quantum dots (QDs) ligated with photochromic molecules has been synthesized and used to study the photomodulation of QD luminescence. The system has been constructed in such a way that the excited-state energies of the QDs and the molecules match but only for one of the conformations of the chromophore, thus enabling phototunable energy transfer from the QD to the ligands. Furthermore, the hybrid system can be immobilized in thin polymer films, creating a solid-state optical switching device. It is demonstrated that the switching of QD photoluminescence between the high-emissive and quenched states occurs on a time scale of tens of milliseconds and in some cases takes even less than 10 ms. The red−green−blue color space can be covered by using three different types of QDs while employing only a single type of photochromic molecule.

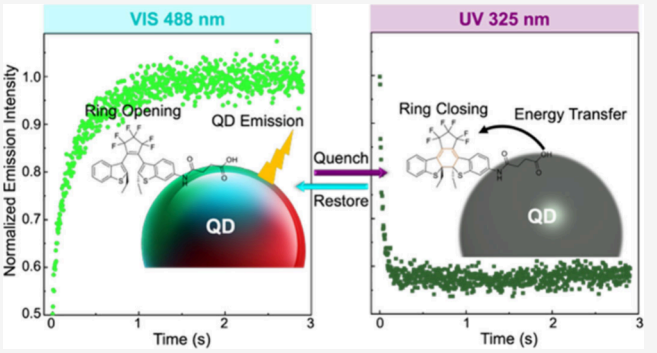


**KEYWORDS:** *semiconductor quantum dots, quantum dot−molecule hybrids, photochromic molecules, photoluminescence modulation, diarylethene photoswitches*



Semiconductor quantum dots (QDs) feature relatively narrow emission spectra that can be tuned across the whole visible spectral range by changing the chemical composition and/or the size of the QDs.[1−8] Together with their robustness against photobleaching and their high fluorescence quantum yields, this makes these materials interesting candidates as sensors[9,10] or as emitters in devices that cover the full red−green−blue (RGB) color space.[11,12] The photoluminescence (PL) from the QDs can be modulated by exploiting Förster resonance energy transfer (FRET) or photoinduced charge transfer (PCT) to organic molecules in close proximity to the QDs.[4,13−16] In this regard, photochromic molecules offer an interesting option because they can be interconverted by light between two bistable conformations, thereby changing the energetic position of their lowest, excited singlet state.[17] Hence, dressing the QDs with photochromic molecules whose excitation energies in the two conformations lie above and below the QD excitation energy allows the spectral overlap between the donor and acceptor moieties to be varied and provides a powerful mechanism to modulate the FRET efficiency. This can be directly observed as a modulation of the PL intensity of the QDs.[12,18−20] Thus, combining the robustness of the QDs with the bistability of the photochromophores offers a promising strategy for designing novel optical units with functionalities that can be controlled by light as an external stimulus.

However, to be truly practical, it is mandatory that the photochromic reaction be (relatively) fast, thermally stable, and fatigue-resistant. Molecules of the 1,2-bis[2-ethylbenzo-[*b*]thiophen-3-yl]-3,3,4,4,5,5-hexafluoro-1-cyclopentenene type (in the following abbreviated as DAE) are known to undergo reversible, ring-closure/ring-opening conformational changes upon illumination with UV/vis light (Figure 1a). Their high fatigue resistance makes them ideal candidates to control photophysical and photochemical reactions.[21−24] There are some reports in the literature about modulating the PL from QDs using photochromic molecules[16,25−27] or molecules of the DAE family in particular.[18,19,28,28−31] However, exploiting such systems for the development of photonic units requires the immobilization of these units in a solid-state environment. To the best of our knowledge, this has not been demonstrated to date, and the works reported to date have all been conducted in solution, making it difficult to realize input/output signal chains between those units. Moreover, in these earlier studies, the time scale required to

Received: December 16, 2025
Revised: February 18, 2026
Accepted: February 19, 2026

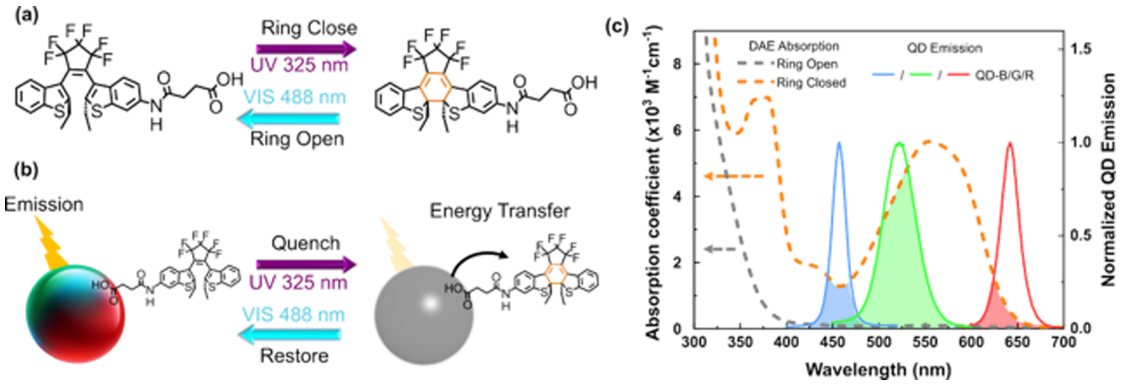


**Figure 1.** (a) Photochromic DAE molecules undergo a photocyclization reaction upon illumination with UV light (purple arrow) and a ring-opening reaction upon illumination with visible light (blue arrow). (b) Schematic illustration of the modulation of the emission from semiconductor quantum dots decorated with carboxylated photochromic DAE molecules as a function of the conformational state of the photoswitches. For DAE in the open state, the QD emits (yellow flash), whereas for DAE in the closed state, QD → DAE excitation energy transfer (black curved arrow) becomes possible, quenching the emission from the QD. For clarity, only one DAE molecule is shown covering the QD. (c) Quantitative absorption spectra of a 0.18 mM solution of DAE in toluene at 21 °C in the open (dashed gray) and closed (dashed orange) conformations. The colored areas show the spectral overlap of the normalized emission spectra from three different types of QDs (QD-B:CdZnS/ZnS, blue; QD-G:$Cd_xZn_{1-x}Se_yS_{1-y}$, green; and QD-R:CdSe/$Cd_xZn_{1-x}S$, red) with absorption spectra of the DAE chromophores in the open state.

observe significant changes of the emitted intensity levels varied between some 10 s and 10 min.[18,29,32] Also, full color range (blue, green, and red) emission modulation in QD:DAE using a single photochromic molecule for blue, green, and red QDs has not been reported.

Here, we address these issues and demonstrate full color modulation of QD PL intensity on time scales as fast as some 10 ms in solid-state thin films.

To achieve this, the DAE molecules are functionalized with carboxylic acid groups, which bind to cationic surface sites on the QDs via simple ligand exchange, as shown in Figure 1b. The synthetic details of the DAE ligands are given in the Supporting Information (Scheme S1). In order to cover the RGB color space, three different types of QDs were used featuring narrow emission bands in the blue, green, and red spectral range. Briefly, core−shell CdZnS/ZnS with an average diameter of 7.73 nm emitting at 455 nm, $Cd_xZn_{1-x}Se_yS_{1-y}$ with an average diameter of 6.82 nm emitting at 515 nm, and core−shell CdSe/$Cd_xZn_{1-x}S$ with an average diameter of 8.82 nm emitting at 640 nm were used; further details are provided in sections 1−3 of the Supporting Information. In the following, these QDs will be referred to as QD-B, QD-G, and QD-R for blue, green, and red, respectively. Since the emission spectra from all three types of QDs feature a reasonable spectral overlap with the absorption spectrum of DAE in the closed state (see Figure 1c), the combined QD:DAE hybrid systems are suited for modulating the excitation energy transfer between the subunits, thereby changing the QD emission intensity between a high and low level. However, before proceeding to solid-state experiments, this strategy is first verified in solution.

In the following, the intensity level obtained from the QDs that is associated with DAE molecules in the open conformation will be referred to as the emissive state, and the intensity level that is associated with the DAE molecules in the closed conformation will be referred to as the quenched state. A single DAE molecule attached to the QD will give only a small effect, whereas above a certain density of adsorbed DAE molecules, these will interact with each other, leading to self-quenching effects among the chromophores. Hence, it seems intuitively clear that there is an optimum ligand surface coverage for maximum modulation of the PL intensity of the QDs. For convenience, the experiments for finding the optimum QD:DAE ratio were carried out in solution and are exemplified below for the case of the QD-G quantum dots (constant QD-G concentration of 40 nM in toluene), for which the QD-G:DAE molar ratio was varied from 1:16 to 1:244. The QD-G emission spectra showed clear differences between the emissive and quenched states as a function of the conformation of the DAE molecules (Figure 2a). Interestingly, the integrated intensities from the emissive state did not change significantly for coverages up to 1:135, whereas the intensities from the quenched state showed a clear decrease as the QD-G:DAE ratio increased from 1:16 to 1:135. However, we observed a decrease in the emissive state intensity of the QD-G at high concentrations of the QD-G:DAE molar ratio above 1:135.

In order to quantify these observations, we define the contrast $C_I$ as the difference in emission intensity between the emissive and quenched state of the QDs, i.e.

$$C_I = \frac{I_{emissive} - I_{quenched}}{I_{emissive}} = 1 - \frac{I_{quenched}}{I_{emissive}} \quad (1)$$

where $I_{emissive}$ and $I_{quenched}$ are the integrated emission intensities of QD-G in the emissive state (associated with DAE in the open-ring conformation) and in the quenched state (associated with DAE in the closed-ring conformation). The resulting integrated emission intensity from QD-G in the emissive and quenched states as a function of the QD-G:DAE ratio is shown in Figure 2b, from which the corresponding contrast is deduced and is shown in Figure 2c. This reveals that the intensity from the emissive state remains nearly constant up to a QD-G:DAE ratio of 1:160 and then drops rapidly for higher coverages. Similarly, the obtainable contrast $C_I$ increases to about 70% for this coverage and then decreases to lower values beyond this coverage. The highest contrast between the emissive and quenched states is found for a QD-G:DAE coverage of about 1:165. The decrease in the contrast for higher coverages may reflect the lower colloidal stability of the QD:DAE systems at higher dye concentrations. If the decrease of the QD emission arises solely from excitation energy


https://doi.org/10.1021/acs.nanolett.5c06282
Nano Lett. XXXX, XXX, XXX−XXX

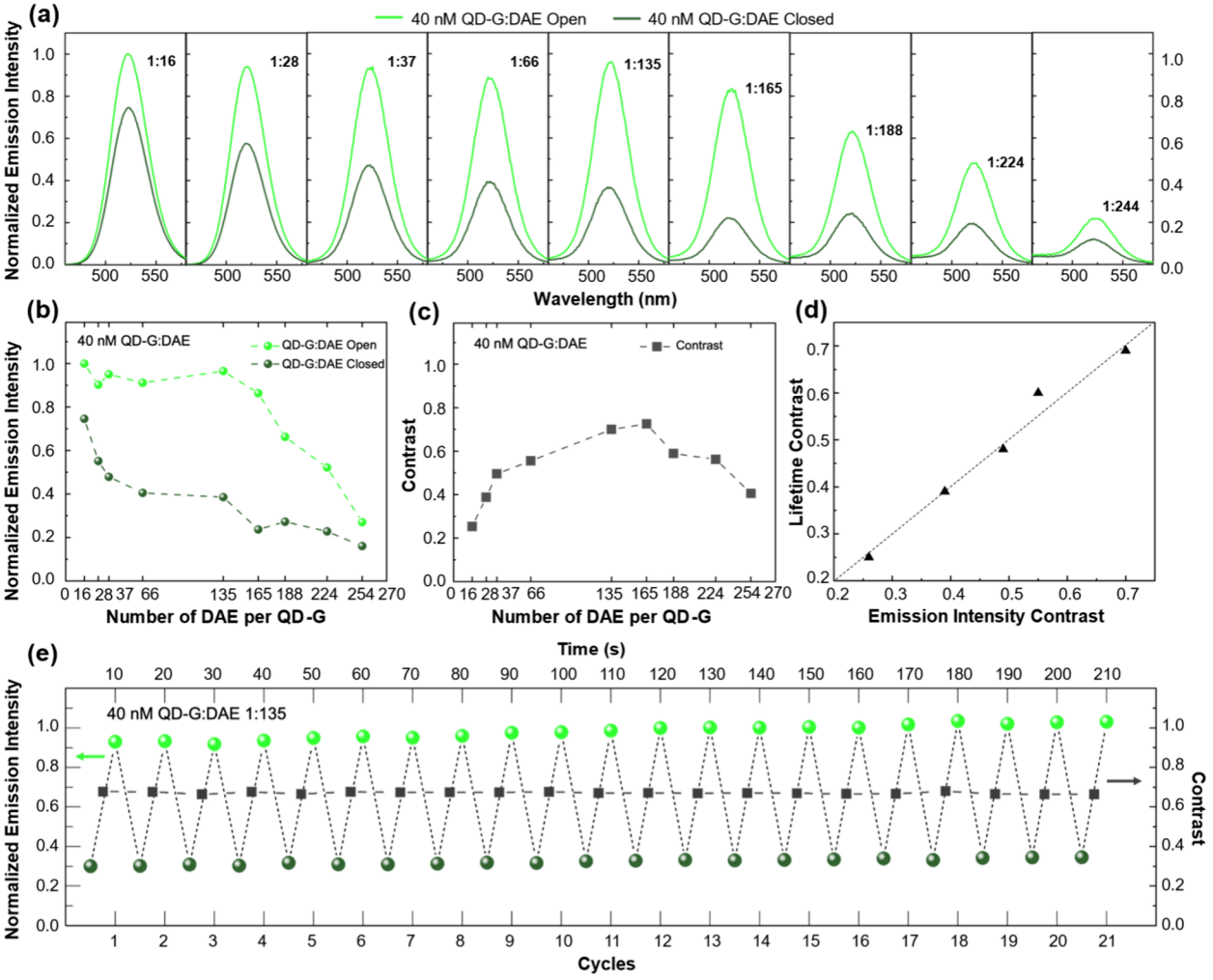


**Figure 2.** (a) Emission spectra of QD-G as a function of the number of adsorbed DAE molecules in the open state (light green) and closed state (dark green). The spectra are peak-normalized to the emission of the 1:16 high-emissive state (green line, first panel), and the coverages, which are given by the number of DAE molecules per QD-G, are indicated in the individual panels. The excitation wavelength was 400 nm, and the concentration of QD-G was 40 nM in toluene. (b) Integrated emission intensity of the QD-G emission in the open state of DAE (light green) and closed state of DAE (dark green). (c) Contrast according to eq 1 between the emissive and quenched state as a function of the ratio of the number of DAE molecules per QD. (d) Relationship between the contrasts $C_I$ and $C_\tau$ for the first five QD-G:DAE coverages. The dotted line has a slope of 1 and serves as a guide for the eye. (e) Integrated emission intensities (green dots, left axis) and contrasts (squares, right axis) for 21 cycles of vis → UV → vis illumination. The UV and vis intensities amounted to 38 mW/cm$^2$ and were applied in alternating ways for 5 s each. The data have been normalized to the highest intensity, and the dashed lines between the data points serve as a guide for the eye.

transfer from the QD to the DAE molecules, without any change in the non-radiative decay channels of the QD, the contrast defined above is equivalent to the FRET efficiency. This efficiency corresponds to the ratio of the QD → DAE energy transfer rate $k_{QD \to DAE}$ and the sum of the intrinsic QD decay rate $k_{QD}$ and the energy transfer rate $k_{QD \to DAE}$, which is equivalent to a lifetime-defined contrast.

$$C_\tau = \frac{k_{QD \to DAE}}{k_{QD} + k_{QD \to DAE}} = 1 - \frac{\tau_{quenched}}{\tau_{emissive}} \quad (2)$$

Determining $C_\tau$ thus requires the fluorescence lifetimes of the QDs in the emissive and quenched states (see section 6 of the Supporting Information). The independently obtained contrasts $C_I$ and $C_\tau$ for the first five QD-G:DAE ratios are compared in Figure 2d and Table S3 of the Supporting Information and show excellent agreement, confirming that the QD emission quenching indeed results from excitation energy transfer to the DAE molecules. This conclusion is in agreement with a rough estimate of the Förster radius based on the photophysical parameters of QD-G and DAE (see section 8 of the Supporting Information). Finally, for the optimum QD-G:DAE coverage of 1:135, the fatigue resistance of the system is demonstrated in Figure 2e, which shows 21 consecutive cycles of vis → UV → vis illumination without any deterioration of the intensity levels or the emission intensity contrast $C_I$ (see also section 9 of the Supporting Information). Similar experiments for QD-B and QD-R likewise yielded optimum QD:DAE coverages of about 1:100 for both species.

The QD:DAE hybrids exhibiting optimum dye ratios in toluene (QD-B:DAE ≈ 1:101, QD-G:DAE ≈ 1:135, and QD-R:DAE ≈ 1:107) were embedded in thin films of PMMA that were prepared by drop casting (see section 1 of the Supporting Information). The reversible switching of the QD emission between the emissive state and the quenched state in PMMA in the solid state is described in detail on the example of the QD-G:DAE system in Figure 3. Figure 3a depicts one


https://doi.org/10.1021/acs.nanolett.5c06282
Nano Lett. XXXX, XXX, XXX−XXX

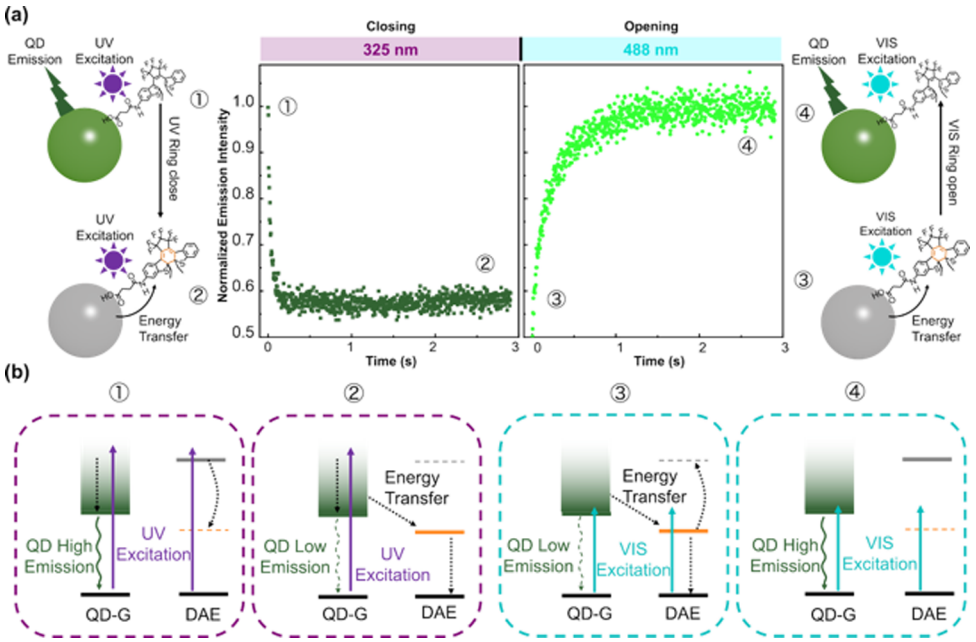


**Figure 3.** (a) (Left) Schematic sketch of the ring-closure reaction of DAE upon UV illumination, ①, enabling excitation energy transfer from QD-G to DAE, ②. (Center) Modulation of the QD emission on the example of the QD-G:DAE hybrid systems embedded in PMMA. The sample is illuminated consecutively for 2.9 s with UV (325 nm, 30 W/cm$^2$) and vis (488 nm, 30 W/cm$^2$) light with a dark period of 0.1 s in between, as indicated by the colored bars at the top. Data points are collected with a bin time of 3.74 ms. Given the different absorption strengths of QD-G and DAE at both wavelengths used, the data in each panel have been normalized (to the highest intensity for the UV illumination and to the averaged highest intensity for the vis illumination) for better comparison. (Right) Schematic sketch of the ring-opening reaction of DAE upon vis illumination, ③, and restoring the emission from the QD-G, ④. To keep things simple, only one DAE molecule linked to the QD-G is shown, and the actual QD-G:DAE ratio was 1:135. (b) Simplified energy level scheme of QD-G and DAE and photophysical processes induced upon UV illumination, ① and ②, and upon vis illumination, ③ and ④.

complete UV−vis illumination cycle for the ring-closure reaction of DAE upon UV illumination, enabling excitation energy transfer from QD-G to DAE, resulting in quenching of the QD emission, and the ring-opening reaction upon vis illumination, restoring the emission of the QD. The corresponding illumination conditions are indicated by the colored bars at the top of the panels. The underlying photophysical processes are illustrated schematically to the left and right of the sequence in Figure 3a and a simplified energy level diagram in Figure 3b for one QD-G and one DAE molecule. Note that the absolute emission intensities for the different laser excitations are not the same due to the different absorption coefficients of QD-G and DAE at each wavelength. Therefore, the data in each panel have been independently normalized to the highest intensity for better comparison. At $t$ = 0, the sample is illuminated with UV light (30 W/cm$^2$), and the emission, initially at a high level, ①, rapidly decreases to a low level, ② (Figure 3a, center). This behavior reflects absorption of the UV radiation by both QD-G and DAE, ① (Figure 3b). While QD-G excitation in the UV leads to strong emission, the UV light simultaneously converts DAE into its closed form (Figure 3a, left), enabling excitation energy transfer from QD-G to DAE, resulting in a gradual decrease of the QD-G PL intensity, ② (Figure 3a and b). Upon switching from UV to vis illumination, the DAE undergoes the ring-opening reaction, ③ (Figure 3a, left, and ③ of Figure 3b). Consequently, the DAE absorption band blue shifts out of resonance with the QD-G absorption, rendering the QD-G → DAE energy transfer inefficient. As a result, the emission from QD-G is restored, ④ (Figure 3a and b).

The time scale of the transition between the emissive and quenched states depends on the intensities of the UV and vis radiation. Therefore, such illumination sequences have been carried out for all three types of QDs as a function of the illumination intensity. Each of the three QD:DAE systems were studied using UV intensities at 325 nm of 1.5, 3, 15, and 30 W/cm$^2$. For the QD-B:DAE system, the vis intensities at 420 nm amounted to 6, 12, 60, and 120 W/cm$^2$. For the other two systems, QD-G:DAE, and QD-R:DAE, the vis intensities at 488 nm were set to 1.5, 3, 15, and 30 W/cm$^2$. The results are shown in Figure 4 from top to bottom for QD-B:DAE (a and b), QD-G:DAE (c and d), and QD-R:DAE (e and f), as a function of the illumination intensities, shown from left to right in each row.

For each QD:DAE system, the top row shows the results under UV illumination (dark color) and the bottom row shows the results under vis illumination (light color). The schematics in the last panel of each of these rows illustrate the illumination conditions as well as the QD emission and quenching processes. For the three types of QDs, the emission intensity initially starts at a high level under UV illumination and then rapidly decreases toward the lower steady-state value (Figure 4a, c, and e). Conversely, under vis illumination, the emission starts at a low intensity and quickly rises to a higher steady-state level, as shown in Figure 4b, d, and f from left to right.

From visual inspection, it is evident that, with increasing illumination intensity, the difference between the initial (high or low) emission level and the steady-state level becomes larger, while the decay (or rise) process itself becomes faster. To quantify the time scale of the transition from the emissive to the quenched state, we define $T_{1/2}$ as the time required to


https://doi.org/10.1021/acs.nanolett.5c06282
Nano Lett. XXXX, XXX, XXX−XXX

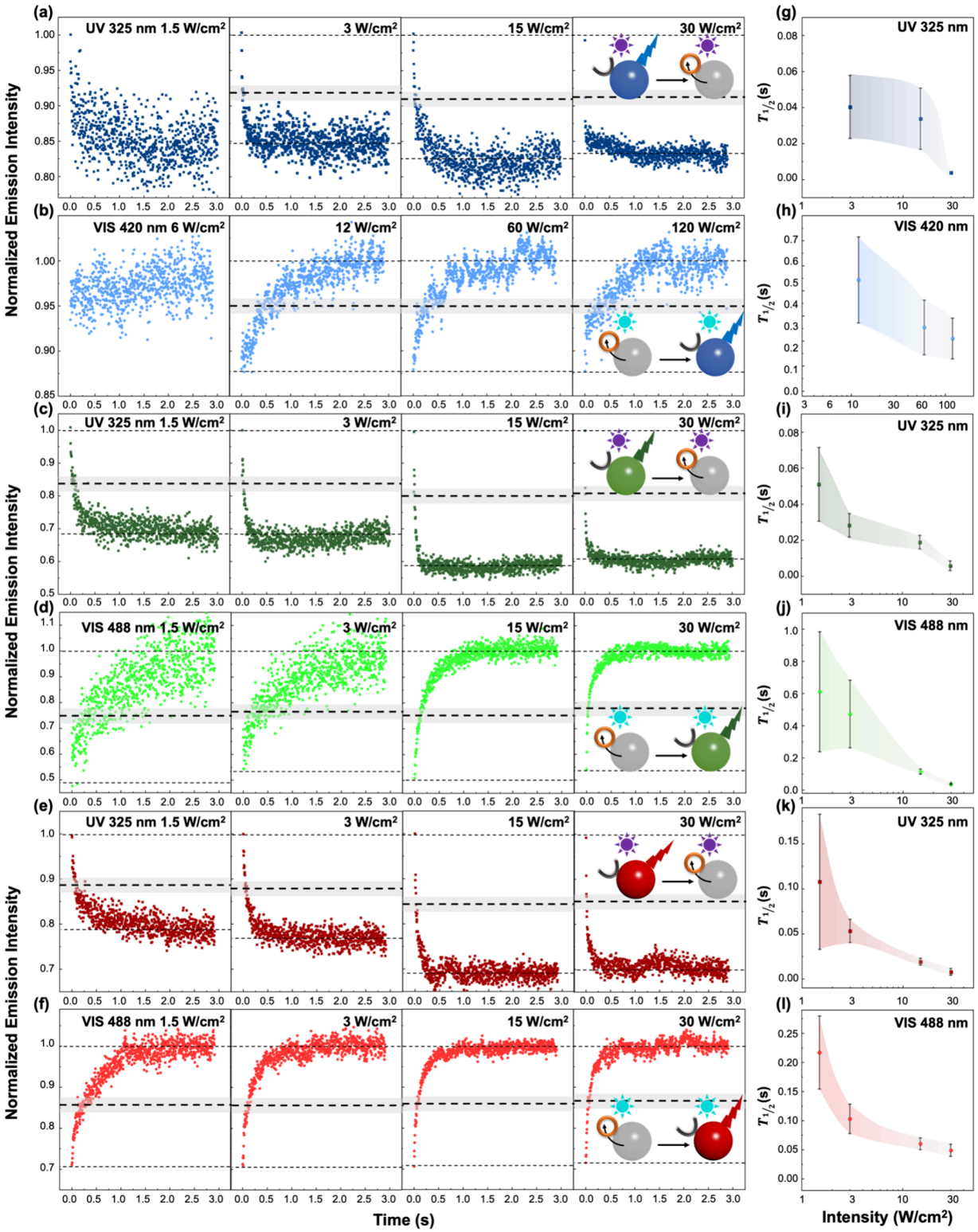


**Figure 4.** Conversion from the high emissive to the quenched state under UV illumination (dark colors) and vice versa under vis illumination (light colors) for (a and b) QD-B:DAE, (c and d) QD-G:DAE, and (e and f) QD-R:DAE in PMMA, as a function of increasing illumination intensities from left to right. The illumination conditions are (a, c, and e) UV, 325 nm, 2.9 s, 1.5, 3, 15, and 30 W/cm$^2$ from left to right; (b) vis, 420 nm, 2.9 s, 6, 12, 60, and 120 W/cm$^2$ from left to right; and (d and f) vis, 488 nm, 2.9 s, 1.5, 3, 15, and 30 W/cm$^2$ from left to right. The data points were acquired every 3.74 ms, which includes a binning time of 2 ms and 1.74 ms for data transfer. Each panel represents a single example from 4 consecutively recorded cycles. For the UV illumination (a, c, and e), the data are normalized to the average of the first data points from the same cycle, as indicated by the dotted lines at the top. For the vis illumination (b, d, and f), the average intensity over the last 0.5 s within each panel serves as a reference level, as indicated by the dotted line at the bottom. The bold dashed line gives the time $T_{1/2}$, required to reach 50% of the difference between the two levels indicated by the two dotted lines. (g–l) $T_{1/2}$ times extracted for the scenario depicted next to the particular panel as a function of the illumination intensity.


https://doi.org/10.1021/acs.nanolett.5c06282
Nano Lett. XXXX, XXX, XXX−XXX

**Table 1. $T_{1/2}$ Times Extracted from Figure 4a–f[a]**

| UV 325 nm intensity (W/cm$^2$) | | 1.5 | 3 | 15 | 30 |
|---|---|---|---|---|---|
| $T_{1/2}$ (ms) | QD-B quenching | N/A | 40 ± 18 | 34 ± 17 | 4* ± 2 |
| | QD-G quenching | 51 ± 21 | 28 ± 7 | 19 ± 4 | 6* ± 3 |
| | QD-R quenching | 108 ± 75 | 53 ± 13 | 19 ± 4 | 8* ± 4 |
| vis 420 nm intensity (W/cm$^2$) | | 6 | 12 | 60 | 120 |
| $T_{1/2}$ (ms) | QD-B restoring | N/A | 443 ± 172 | 254 ± 109 | 209 ± 81 |
| vis 488 nm intensity (W/cm$^2$) | | 1.5 | 3 | 15 | 30 |
| $T_{1/2}$ (ms) | QD-G restoring | 610 ± 386 | 471 ± 210 | 113 ± 16 | 36 ± 3 |
| | QD-R restoring | 217 ± 62 | 103 ± 25 | 60 ± 10 | 49 ± 10 |

[a]For QD-B, the data for the lowest intensities were too noisy for obtaining a meaningful result. The asterisks mark temporal decays that occurred within one or two data points.

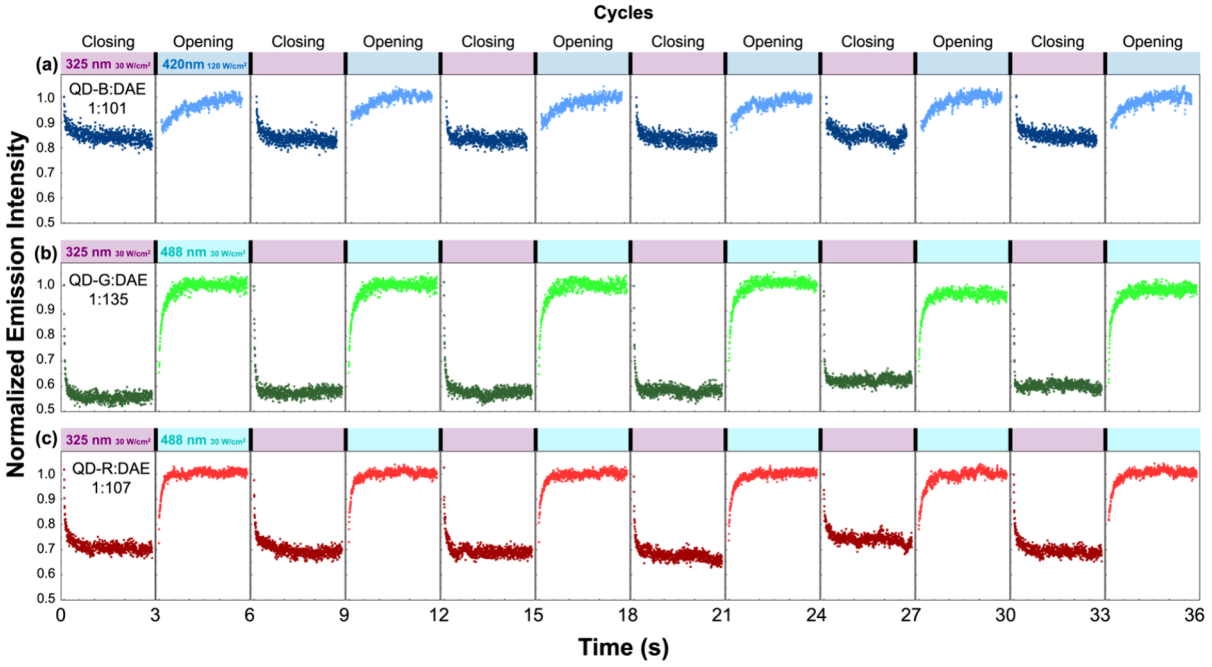


**Figure 5.** Modulation of the QD emission of QD-DAE hybrid systems embedded in PMMA was recorded for 6 consecutive illumination cycles. For each type of QD, the QD:DAE ratio that gave the optimum contrast has been used and is indicated in the figure. The samples are illuminated alternatingly for 2.9 s with UV and vis light with a dark period of 0.1 s in between, as indicated by the colored bars at the top. Data points are collected with a bin time of 3.74 ms. As before, the data in the individual panels have been normalized (to the highest intensity for the UV illumination and to the averaged highest intensity for the vis illumination) for better comparison. (a) QD-B:DAE; UV, 325 nm, 30 W/cm$^2$; vis, 420 nm, 120 W/cm$^2$. (b) QD-G:DAE; UV, 325 nm, 30 W/cm$^2$; vis, 488 nm, 30 W/cm$^2$. (c) QD-R:DAE; UV, 325 nm, 30 W/cm$^2$; vis, 488 nm, 30 W/cm$^2$. Note that the absorption strength of DAE is different at 420 nm (used for QD-B) and 488 nm (used for QD-G and QD-R).

reach 50% of the difference between the initial level and the average steady-state level. The extracted values of $T_{1/2}$ as a function of illumination intensities are shown in Figure 4g, h, and i for the various scenarios and are also summarized in Table 1. For all three QD:DAE systems, the conversion times decrease monotonically with an increasing illumination intensity in both conversion directions. Moreover, all conversion times are shorter than 1 s and can be as short as 10 ms, at the highest illumination intensities, especially for the quenching process using UV illumination. For lower illumination intensities, the conversion slows down to 2 s (at 38 mW/cm$^2$) and 6 s (at 3.8 mW/cm$^2$) [see Figure S12 (section 9 of the Supporting Information)].

In Figure 5, sequences of 6 UV and vis illumination cycles for the three QD:DAE systems are shown. For the three types of QDs, the illumination cycles give qualitatively the same result, and all of them feature a high degree of reproducibility without any sign of deterioration. The long-term stability was tested over 220 cycles using the QD-G:DAE system as a testbed without showing any signs of fatigue [see Figure S13 (section 10 of the Supporting Information)]. The modulation depths, i.e., the intensity difference between the emissive state and the quenched state, are largest for the QD-G system, which reflects the fact that the emission spectra of these QDs exhibit the largest spectral overlap with the absorption spectrum of the closed DAE molecules (see Figure 1c).

Finally, we tested the thermal back reaction using the QD-G:DAE system [Figure S14 (section 11 of the Supporting Information)]. The sample was initialized in the emissive state (QD-G:DAE, open) and subsequently quenched with UV illumination until a steady state was reached. Then, the sample was kept in a water bath at 40 °C in the dark for 24 h. After that time, the emission was remeasured, and a transition back to the emissive state was not observable.

In summary, it has been demonstrated that a single type of photochromic molecule can be employed to reversibly


https://doi.org/10.1021/acs.nanolett.5c06282
Nano Lett. XXXX, XXX, XXX−XXX

modulate the PL of three different types of QDs between an emissive and quenched state in the solid phase, enabling system integration. The selected QDs span the RGB color space. A modulation contrast of up to 70% has been achieved on a sub-millisecond time scale in a solid-state device.

This work might become relevant for engineering-oriented material optimization studies for promoting quantum dot–photochromic molecule hybrids as versatile building blocks for integrated, light-addressable, optically switchable photonic devices.

## ■ ASSOCIATED CONTENT

### Supporting Information

The Supporting Information is available free of charge at https://pubs.acs.org/doi/10.1021/acs.nanolett.5c06282.

Materials and methods, size distributions of semiconductor quantum dots, UV–vis spectra of semiconductor quantum dots, verification of the modulation of the QD PL in solution, analysis of the QD:DAE ratio, fluorescence lifetimes and FRET efficiency, QD-G photoluminescence quantum yield, plausibility check of excitation energy transfer from QD to DAE, switching behavior for low illumination intensities, long-term stability, and thermal back reaction (PDF)

## ■ AUTHOR INFORMATION


### Corresponding Author

**Jürgen Köhler** − *Spectroscopy of Soft Matter, University of Bayreuth, 95440 Bayreuth, Germany; Bavarian Polymer Institute, University of Bayreuth, 95440 Bayreuth, Germany; Bayreuth Institute for Macromolecular Research (BIMF), 95440 Bayreuth, Germany;* orcid.org/0000-0002-4214-4008; Email: juergen.koehler@uni-bayreuth.de

### Authors

**Heyou Zhang** − *Spectroscopy of Soft Matter, University of Bayreuth, 95440 Bayreuth, Germany;* orcid.org/0000-0001-9513-3874

**Pankaj Dharpure** − *Applied Functional Materials, University of Bayreuth, 95440 Bayreuth, Germany*

**Arun Ashokan** − *ARC Centre of Excellence in Exciton Science, School of Chemistry, University of Melbourne, Parkville, Victoria 3010, Australia;* orcid.org/0000-0002-0641-3995

**Max Gießübel** − *Spectroscopy of Soft Matter, University of Bayreuth, 95440 Bayreuth, Germany*

**Paul Mulvaney** − *ARC Centre of Excellence in Exciton Science, School of Chemistry, University of Melbourne, Parkville, Victoria 3010, Australia;* orcid.org/0000-0002-8007-3247

**Mukundan Thelakkat** − *Applied Functional Materials and Bavarian Polymer Institute, University of Bayreuth, 95440 Bayreuth, Germany; Bayreuth Institute for Macromolecular Research (BIMF), 95440 Bayreuth, Germany;* orcid.org/0000-0001-8675-1398

Complete contact information is available at: https://pubs.acs.org/10.1021/acs.nanolett.5c06282


### Notes

The authors declare no competing financial interest.

## ■ ACKNOWLEDGMENTS

J.K., M.G., and M.T. thankfully acknowledge financial support by the Deutsche Forschungsgemeinschaft (GRK 2818) and the Bavarian State Ministry for Arts and Science within the initiative “Solar Technologies Go Hybrid”. H.Z. thanks the Deutscher Akademischer Austauschdienst (PPP 57750753), P.M. thanks the ARC for support through CE170100026.

## ■ REFERENCES


(1) Elimelech, O.; Aviv, O.; Oded, M.; Banin, U. A Tale of Tails: Thermodynamics of CdSe Nanocrystal Surface Ligand Exchange. *Nano Lett.* **2020**, *20*, 6396−6403.

(2) Pun, A. B.; Mule, A. S.; Held, J. T.; Norris, D. J. Core/Shell Magic-Sized CdSe Nanocrystals. *Nano Lett.* **2021**, *21*, 7651−7658.

(3) Chen, Z.; Manian, A.; Widmer-Cooper, A.; Russo, S. P.; Mulvaney, P. Semiconductor Quantum Dots in the Cluster Regime. *Chem. Rev.* **2025**, *125*, 4359−4396.

(4) Muhammad, H.; Masab, M.; Ullah, N.; Yasmeen, K.; Majeed Khan, A.; Tuzen, M.; Saleh, T. A. A comprehensive review of current trends and future perspective of quantum dots regarding their optical and photoswitchable properties. *Renewable and Sustainable Energy Reviews* **2025**, *223*, 115984.

(5) Rempel, A. A.; Ovchinnikov, O. V.; Weinstein, I. A.; Rempel, S. V.; Kuznetsova, Y. V.; Naumov, A. V.; Smirnov, M. S.; Eremchev, I. Y.; Vokhmintsev, A. S.; Savchenko, S. S. Quantum dots: Modern methods of synthesis and optical properties. *Russ. Chem. Rev.* **2024**, *93*, RCR5114.

(6) Wegner, K. D.; Resch-Genger, U. The 2023 Nobel Prize in Chemistry: Quantum dots. *Anal. Bioanal. Chem.* **2024**, *416*, 3283−3293.

(7) Rabouw, F. T.; de Mello Donega, C. Excited-State Dynamics in Colloidal Semiconductor Nanocrystals. *Topics in Current Chemistry* **2016**, *374*, 58.

(8) Murray, C. B.; Kagan, C. R.; Bawendi, M. G. Synthesis and Characterization of Monodisperse Nanocrystals and Close-Packed Nanocrystal Assemblies. *Annu. Rev. Mater. Sci.* **2000**, *30*, 545−610.

(9) Gierschner, J.; Shi, J.; Milián-Medina, B.; Roca-Sanjuán, D.; Varghese, S.; Park, S. Luminescence in Crystalline Organic Materials: From Molecules to Molecular Solids. *Adv. Optical Mater.* **2021**, *9*, 2002251.

(10) Somers, R. C.; Bawendi, M. G.; Nocera, D. G. CdSe nanocrystal based chem-/bio- sensors. *Chem. Soc. Rev.* **2007**, *36*, 579−591.

(11) Pietryga, J. M.; Park, Y.-S.; Lim, J.; Fidler, A. F.; Bae, W. K.; Brovelli, S.; Klimov, V. I. Spectroscopic and Device Aspects of Nanocrystal Quantum Dots. *Chem. Rev.* **2016**, *116*, 10513−10622.

(12) Hildebrandt, N.; Spillmann, C. M.; Algar, W. R.; Pons, T.; Stewart, M. H.; Oh, E.; Susumu, K.; Díaz, S. A.; Delehanty, J. B.; Medintz, I. L. Energy Transfer with Semiconductor Quantum Dot Bioconjugates: A Versatile Platform for Biosensing, Energy Harvesting, and Other Developing Applications. *Chem. Rev.* **2017**, *117*, 536−711.

(13) Issac, A.; Al-Maskari, S.; Sofin, R. S.; Ibrahim, A. R.; Abou-Zied, O. K. Photoexcited Charge Trapping Induced Quenching of Radiative Recombination Pathways in CuInS2/ZnS-Dye Nanoassemblies. *J. Lumin.* **2021**, *239*, 118402.

(14) Al-Maskari, S.; Issac, A.; Varanasi, S. R.; Hildner, R.; Sofin, R. G. S.; Ibrahim, A. R.; Abou-Zied, O. K. Dye-induced photoluminescence quenching of quantum dots: Role of excited state lifetime and confinement of charge carriers. *Physical chemistry chemical physics: PCCP* **2023**, *25*, 14126−14137.

(15) Wu, N.; Kirkwood, N.; Neto, N. S.; Pervin, R.; Mulvaney, P.; Wong, W. W. H. Energy Transfer between CdZnS Quantum Dots and Perylene Diimide Dyes. *J. Phys. Chem. C* **2023**, *127*, 2116−2126.

(16) Budyka, M. F.; Nikulin, P. A.; Gavrishova, T. N.; Chashchikhin, O. V. Photomodulation of a Dual-Color Luminescent System Combining Quantum Dots with a FRET Acceptor Ligand**. *ChemPhotoChem.* **2021**, *5*, 582−590.

(17) Irie, M.; Fukaminato, T.; Matsuda, K.; Kobatake, S. Photochromism of diarylethene molecules and crystals: memories, switches, and actuators. *Chem. Rev.* **2014**, *114*, 12174−12277.
(18) Díaz, S. A.; Gillanders, F.; Jares-Erijman, E. A.; Jovin, T. M. Photoswitchable semiconductor nanocrystals with self-regulating photochromic Förster resonance energy transfer acceptors. *Nat. Commun.* **2015**, *6*, 6036.
(19) Seto, Y.; Yamada, R.; Kitagawa, D.; Kim, D.; Kobatake, S. Photoluminescence ON/OFF Switching of CdSe/ZnS Core/Shell Quantum Dots Coated with Diarylethene Ligands. *Chem. Lett.* **2019**, *48*, 1394−1397.
(20) Mokhtar, A.; Morinaga, R.; Akaishi, Y.; Shimoyoshi, M.; Kim, S.; Kurihara, S.; Kida, T.; Fukaminato, T. Reversible Luminescence Photoswitching of Colloidal CsPbBr 3 Nanocrystals Hybridized with a Diarylethene Photoswitch. *ACS Materials Lett.* **2020**, *2*, 727−735.
(21) Berberich, M.; Krause, A.-M.; Orlandi, M.; Scandola, F.; Würthner, F. Toward fluorescent memories with nondestructive readout: photoswitching of fluorescence by intramolecular electron transfer in a diaryl ethene-perylene bisimide photochromic system. *Angew. Chem., Int. Ed.* **2008**, *47*, 6616−6619.
(22) Berberich, M.; Würthner, F. Terrylene bisimide-diarylethene photochromic switch. *Chem. Sci.* **2012**, *3*, 2771−2777.
(23) Berberich, M.; Natali, M.; Spenst, P.; Chiorboli, C.; Scandola, F.; Würthner, F. Nondestructive Photoluminescence Read-Out by Intramolecular Electron Transfer in a Perylene Bisimide-Diarylethene Dyad. *Chem. - Eur. J.* **2012**, *18*, 13651−13664.
(24) Andréasson, J.; Pischel, U. Light-stimulated molecular and supramolecular systems for information processing and beyond. *Coordin. Chem. Rev.* **2021**, *429*, 213695.
(25) Chashchikhin, O. V.; Budyka, M. F.; Gavrishova, T. N.; Nikulin, P. A. Photoactive hybrid nanosystem based on CdS quantum dot and novel diarylethylene photochrome as FRET acceptor. *Chem. Phys. Lett.* **2018**, *696*, 135−138.
(26) Padgaonkar, S.; Eckdahl, C. T.; Sowa, J. K.; López-Arteaga, R.; Westmoreland, D. E.; Woods, E. F.; Irgen-Gioro, S.; Nagasing, B.; Seideman, T.; Hersam, M. C.; et al. Light-Triggered Switching of Quantum Dot Photoluminescence through Excited-State Electron Transfer to Surface-Bound Photochromic Molecules. *Nano Lett.* **2021**, *21*, 854−860.
(27) Barachevsky, V. A.; Venidiktova, O. V.; Valova, T. M.; Gorelik, A. M.; Vasiliev, R. B.; Khuzin, A. A.; Tuktarov, A. R.; Karpach, P. V.; Stsiapura, V. I.; Vasilyuk, G. T.; et al. Photochromic systems with photoinduced emission modulation of colloidal CdSe quantum wells. *Photochem. Photobiol. Sci.* **2019**, *18*, 2661−2665.
(28) Jiang, G.; Jia, Y.; Cui, S.; Pu, S. Photo-Modulated Reversible Switching of Fluorescence from ZnO Quantum Dots with a Photochromic Diarylethene. *ChemistrySelect* **2020**, *5*, 13919−13924.
(29) Scherbovich, A. A.; Maskevich, S. A.; Karpach, P. V.; Vasilyuk, G. T.; Stsiapura, V. I.; Venidiktova, O. V.; Ayt, A. O.; Barachevsky, V. A.; Khuzin, A. A.; Tuktarov, A. R.; et al. Reversible Photoinduced Luminescence Modulation from Nanospheres Containing CdSe/ZnS Quantum Dots and Photochromic Diarylethene. *J. Phys. Chem. C Nanomater Interfaces* **2020**, *124*, 27064−27070.
(30) Yamamoto, M.; Morimoto, M.; Irie, M.; Eguchi, D.; Tamai, N. Deciphering the Optical Switching Mechanism of CdSe/CdS QDs Luminescence by Diarylethene Molecular Photoswitches: A Stochastic Model Analysis. *J. Phys. Chem. C Nanomater Interfaces* **2024**, *128*, 19758−19766.
(31) Yano, N.; Yamauchi, M.; Kitagawa, D.; Kobatake, S.; Masuo, S. Photoluminescence On/Off Switching of a Single Colloidal Quantum Dot Using Photochromic Diarylethene. *J. Phys. Chem. C* **2020**, *124*, 17423−17429.
(32) Díaz, S. A.; Giordano, L.; Azcárate, J. C.; Jovin, T. M.; Jares-Erijman, E. A. Quantum dots as templates for self-assembly of photoswitchable polymers: Small, dual-color nanoparticles capable of facile photomodulation. *J. Am. Chem. Soc.* **2013**, *135*, 3208−3217.


https://doi.org/10.1021/acs.nanolett.5c06282
*Nano Lett.* XXXX, XXX, XXX−XXX